LAWRENCE
LIVERMORE
NATIONAL
LABORATORY

LLNL-JRNL-475802

ALD Functionalized Nanoporous Gold: Thermal Stability, Mechanical Properties, and Catalytic Activity

M. M. Biener, J. Biener, A. Wichmann , A. Wittstock, T. F. Baumann, M. Baeumer, A. V. Hamza

March 24, 2011

Nanoletters

Disclaimer

ALD Functionalized Nanoporous Gold: Thermal Stability, Mechanical Properties, and Catalytic Activity

Monika M. Biener,[*,1] *Juergen Biener,*[1] *Andre Wichmann,*[2] *Arne Wittstock,*[2] *Theodore F. Baumann,*[1] *Marcus Bäumer*[2] *and Alex V. Hamza*[1]

[1)] Nanoscale Synthesis and Characterization Laboratory, Lawrence Livermore National Laboratory, 7000 East Ave, Livermore, CA 94550

[2)] Institute of Applied and Physical Chemistry, University Bremen, Bremen, Germany

[*] Corresponding author: Biener3@llnl.gov

Nanoporous metals have many technologically promising applications but their tendency to coarsen limits their long-term stability and excludes high temperature applications. Here, we demonstrate that atomic layer deposition (ALD) can be used to stabilize and functionalize nanoporous metals. Specifically, we studied the effect of nanometer-thick alumina and titania ALD films on thermal stability, mechanical properties, and catalytic activity of nanoporous gold (np-Au). Our results demonstrate that even only one-nm-thick oxide films can stabilize the nanoscale morphology of np-Au up to 1000°C, while simultaneously making the material stronger and stiffer. The catalytic activity of np-Au can be drastically increased by TiO_2 ALD coatings. Our results open the door to high temperature sensor, actuator, and catalysis applications and functionalized electrodes for energy storage and harvesting applications.

KEYWORDS: nanoporous gold, alumina, titania, atomic layer deposition, core-shell structures, nanoindentation, catalysis

Nanoporous metals such as nanoporous gold (np-Au) prepared by dealloying have recently attracted considerable interest fueled by their potential use in catalysis[1-6], sensor[3, 7-12] and actuator applications.[13-15] The remarkable properties of these materials are a consequence of their characteristic bicontinuous nanoporous structure of interconnected nm-sized pores and ligaments that is formed by a self-organization process.[16, 17] A disadvantage of this nanoscale morphology in the context of applications is that it is thermodynamically unstable and prone to coarsening.[10, 18, 19] For example, the length scale of both ligaments and pores of np-Au increases by more than two orders of magnitude by heating the material to 800°C.[18] Coarsening severely limits the practical applications of np-Au as it leads, for example, to a loss of catalytically active surface and reduces the mechanical strength[20] that is important for the actuator application. Consequently, several strategies have been tested to increase the thermal stability of this material. For example, the stability can be improved by adding small amounts of high melting point metals such as Pd[7] and Pt,[21, 22] or by using surface chemistry to suppress surface diffusion.[23] But even 'stabilized' np-Au has only limited thermal stability as, for example, annealing of Pt-stabilized np-Au leads to severe coarsening at 400 °C,[24] and stabilizing surface oxygen starts to desorb around 200 °C.[23]

In the present study we explore the potential of atomic layer deposition (ALD) to improve the thermal stability and mechanical properties of *bulk* np-Au beyond the currently achieved temperature regions which, for example, could open the door to high temperature sensor and actuator applications.[13-15] At the same time, our study aims at elucidating whether the deposition of an oxide on the inner surfaces of np-Au can also boost its catalytic properties as it is known that the combination of Au and reducible oxide, such as titania, leads to highly active catalysts.[25] Combined with an increased thermal stability this could enable high temperature catalytic applications of np-Au that are not yet possible. ALD is ideally suited to apply nanometer thick, uniform and conformal coatings to high aspect ratio materials such as bulk np-Au.[26-28] ALD is also a wafer-compatible technology and thus could be used to modify wafer-supported np-Au films.[29] Qian *et al*.[30, 31] first successfully used ALD to tune the optical properties of 100-nm-thick np-Au films by partially or completely filling the pores with Al_2O_3. In the present study we selected Al_2O_3 for its thermal stability,[32, 33] and TiO_2 for its potential to add functionality for catalytic, photocatalytic, solar energy harvesting, and energy storage applications.[34-37] For example, ALD TiO_2 thin films can be used as active cathode material in nanostructured Li-ion batteries,[37] and TiO_2 nanoparticle decorated np-Au is an efficient electrode material for photocatalytic oxidation of methanol.[36]

Our experiments reveal that even only one-nm-thick Al_2O_3 films can stabilize the nanoscale morphology of nanoporous gold up to 1000°C, i.e. close to the melting point of bulk gold (1064 °C), while making the material stronger and stiffer. The thermal stability of TiO_2-coated np-Au is lower than that of Al_2O_3-coated np-Au, but still much higher than that of the uncoated material. Here, annealing transforms the initial uniform and continuous TiO_2 layer into highly dispersed TiO_2 nanoparticles which increases the catalytic activity of np-Au for CO oxidation by almost 300%.

Disk-shaped samples of np-Au (diameter ~5 mm, thickness 200-300 microns) with a porosity of ~ 70% were prepared by selective dissolution (dealloying) of $Ag_{0.7}Au_{0.3}$ alloy samples in concentrated nitric acid (48 hrs, ~65 wt% HNO_3) as described previously.[39] The average

ligament diameter for each sample was determined from ligament diameter distributions that were obtained by geometrical evaluation (i.e., measuring the diameter of randomly selected ligaments at their center point). These average values are those displayed in Figure 2a. The ligament diameter of the as-prepared material is ~54 nm, and its specific surface area is ~3.6 m^2/g.

Nanometer-thick Al_2O_3 and TiO_2 films were deposited by ALD using the well-established trimethyl-aluminum ($AlMe_3/H_2O$)[28] and titanium tetrachloride ($TiCl_4/H_2O$)[40] ALD processes in a warm wall reactor (wall and stage temperature of 125 ^oC for Al_2O_3 and 110 ^oC for TiO_2). Both ALD processes are ideally suited to coat high aspect ratio materials such as bulk np-Au to the high volatility of the $AlMe_3$ and $TiCl_4$ precursors, and the low process temperature.[40, 41] Long pulse, pump and purge times (90 s each) were used to ensure uniform coatings throughout the porous material. Static conditions were used for $AlMe_3$, $TiCl_4$, and H_2O pulses, during which the chamber was isolated from the vacuum line. The film thickness was controlled by adjusting the number of ALD cycles (2-30), and the growth rate per cycle was calculated from the measured mass gain, the known surface area of np-Au, and densities of ALD Al_2O_3 and TiO_2.

The morphology and composition of the ALD-modified np-Au samples was characterized by Scanning Electron Microscopy and Energy Dispersive Spectroscopy (SEM/EDAX). Coarsening of np-Au during annealing (2h/400-1000 ^oC/air) was assessed by cross-sectional SEM (XSEM). The mechanical properties (Young's modulus and hardness) were studied by conventional load-controlled nanoindentation using a Berkovich tip. Nanoindentation tests were performed on polished samples (polished before dealloying) using a constant loading rate of 500 μN/s with loads ranging from 200 to 5000 μN. A minimum of 49 indents was made on each sample, and the standard Oliver-Pharr method [42] was used to determine modulus and hardness values from the load-displacement curves. The catalytic performance was evaluated using a continuous (plug-flow) reactor made of a quartz glass tube (inner diameter ~ 1.5 cm) which was placed in an electrical oven for temperature control. The inlet gas stream consisted of a mixture of 4-20 vol. % CO (*Linde*, 4.7) and 30 vol. % O_2 (*Linde,* 5.0) using He (*Linde*, 5.0) as a carrier gas (total flow set to 50 sccm). The gas composition at the reactor exit was analyzed online by an IR-Gas-Analyzer (URAS 10E, Hartmann und Braun).

For both ALD processes, the normalized mass gain increased approximately linear with the number of ALD cycles (Figure 1). The Al_2O_3 growth rate is ~0.25 nm per cycle assuming a density[41] of ~2.8 g/cm^3 and a specific surface area of ~3.6 m^2 per gram np-Au (estimated from the ligament diameter of ~54 nm). This is approximately twice the value of the growth rate reported in the literature (0.125 nm per cycle at 125^oC),[41] which suggests some CVD contribution due to incomplete purging of the reactants trapped in the nanometer scale pores of our 200-300 μm thick samples (pore length/pore diameter > 10^3). This, however, did not affect the uniformity of our samples as cross-sectional EDAX analysis confirmed the uniformity of the alumina coating across the sample cross section. Higher deposition rates (0.15-0.3 nm Al_2O_3 per cycle) have also been observed for much thinner, 100-nm-thick np-Au films.[30, 31] For titania, we observed a deposition rate of ~0.07 nm per cycle, consistent with the value reported in the literature (0.078 nm per cycle at 100^oC).[40]

Improving the thermal stability of np-Au is very important for many potential applications in the fields of catalysis, sensorics and actuation as it opens the door for higher operating temperatures and increases the long term stability of the material. Our results demonstrate that

nm-thick ALD coatings can effectively suppress coarsening of the nanoscale structure of np-Au thus preserving its high surface area. The results regarding annealing experiments on as-prepared and alumina-coated np-Au samples are summarized in Figure 2a-e. The annealing behavior of uncoated samples is similar to that published in previous work,[10, 18, 19] and demonstrates the thermal instability of this nanostructured material. The ligaments coarsen rapidly with increasing annealing temperature, for example, from 54±12 nm (as-prepared) to 630±130 and 2850±850 nm after annealing at 600 and 900 °C, respectively (Figure 2a). ALD coating with Al_2O_3 at 125 °C did only marginally increase of the characteristic length scale of the as-prepared material from 54 to 56 nm. Once the material is coated, however, it is stable up to at least 900 °C which is almost 90% of the melting temperature of bulk gold. Even samples annealed at 1000 °C still show the original nanoporous structure (Figure 2e), but the finding that larger, well-facetted micrometer-sized Au crystals now decorate the outer surface of the np-Au sample (Figure 2d) suggests that Au starts to diffuse out of the alumina-coated Au ligaments. Interestingly, the breakdown of the stabilizing effect of the Al_2O_3 coating coincides with the crystallization temperature of the initially amorphous Al_2O_3 film.[32, 33]

In one instance, we found several empty alumina 'shells' in a sample that was annealed at 600 °C. This finding demonstrates two important points: (1) even few-nm-thick ALD alumina films are continuous, and (2) defects in the alumina coating drastically reduce the thermal stability. The thickness of the alumina films, on the other hand, does not seem to have a pronounced effect on the thermal stability, and even samples that were coated with sub-nm-thick alumina films (2 ALD cycles) were stable up to at least 900 °C.

The mechanical behavior of np-Au is, for example, crucial for its actuator[13, 43] application where it controls the maximum stress that can be applied by the actuator. Here, we use nanoindentation to assess the mechanical properties of ALD-coated np-Au. Our results demonstrate that Al_2O_3 coatings make np-Au harder and stiffer which is summarized in Figure 3. As expected, both elastic modulus (Figure 3c) and hardness (Figure 3d) increase with increasing number of ALD cycles. Both hardness and stiffness further increase upon annealing at 600 °C (Figure 3b). The latter effect can be attributed to the densification of amorphous alumina films that occurs around this temperature.[32] Crystallization, on the other hand, requires much higher annealing temperatures of ~1000 °C.[32, 33]

In an attempt to better understand the effect of ALD coatings on the mechanical behavior of np-Au, we first applied the core-shell model developed by Liu et al. [44] to estimate the mechanical behavior of the Al_2O_3-coated gold ligaments, and then used these values as an input to the Gibson-Ashby (G-A) scaling equations[45] that correlate the properties of the individual ligaments with the bulk mechanical response of np-Au as measured by nanoindentation experiments.[20, 39, 46, 47] According to the G-A scaling equations, the Young's modulus E^* and yield strength σ^* of np-Au are related to the Young's modulus E_s and yield strength σ_s of the individual ligaments by

$$E^* = C_1 E_s \left(\frac{\rho^*}{\rho_s}\right)^{n_1} \quad (1) \quad and \quad \sigma^* = C_2 \sigma_s \left(\frac{\rho^*}{\rho_s}\right)^{n_2} \quad (2)$$

where ρ^*/ρ_s is the relative density of the material (0.3 in the present study). The proportionality constants C_1 and C_2 describe the cell geometry and the density exponents n_1 and n_2 depend on the elastic/plastic cell deformation mechanism. Experimental data obtained from macroscopic

open-cell foam materials are usually well fitted by using $C_1=1/n_1=2$ and $C_2=0.3/n_2=3/2$, respectively.[45] In the case of np-Au, however, a density exponent n_1 of 2 seems to underestimate the density dependence of E^*.[47] Here, we assume a value of $n_1=3$ that better describes the experimentally observed density dependence.[47]

According to Liu *et al.* [44] the Young's modulus of core-shell structures depends on both the Young's modulus (E_{core} and E_{shell}) as well as on the fractional volumes (V_{core}/V and V_{shell}/V) of core and shell via

$$E_s = \frac{V_{core}}{V} E_{core} + \frac{V_{shell}}{V} E_{shell} \qquad (3)$$

where V_{core}, V_{shell} and V are the volume of the core, shell, and core plus shell, respectively. E_s can then be calculated from the normalized mass gain data shown in Figure 1 using the Young's modulus of Au single crystals (57–85 GPa)[48] and ALD alumina films (150 GPa)[49, 50] as reference. Inserting Eq. (3) into Eq. (1) then yields the predicted lower and upper bounds of E^* of the Al_2O_3-coated np-Au (red lines in Figure 3c). This simple model describes the experimental data relatively well, although it predicts too high values for thicker ALD films. To check if the mechanical response of Al_2O_3-coated np-Au is simply the sum of its components, the Au core and the alumina shell, we also tested the mechanical properties of a free-standing alumina shell structure prepared by removing the Au core from a np-Au sample coated with 10 Al_2O_3 ALD cycles (details of the preparation and the mechanical properties will be described in an oncoming publication). The modulus of uncoated np-Au and the free-standing alumina shell are 1.83±0.08 GPa and 0.14 GPa, repectively. It is clear that the sum of these components (blue data point in Figure 3c) severely underestimates the effect of the Al_2O_3 coating on the Young's modulus of np-Au. In fact, the measured increase in the Young's modulus is almost 10 times the Young's modulus of the free-standing Al_2O_3 foam.

In analogy to Eq. (3), we also calculated the yield strength σ_s of Al_2O_3-coated Au ligaments using the yield strength of 50 nm Au ligaments (~1.1 GPa, obtained by applying Eq. (2) to uncoated np-Au)[20, 39] and ALD alumina (~2.7 GPa, σ = nanoindentation hardness/3)[49] as reference. Insertion in Eq (2) then yields the predicted yield strength of Al_2O_3-coated np-Au shown as red line in Figure 3d. Although the agreement between experiment and model is reasonable for thin coatings, the experimentally observed strengthening of thicker films is severely underestimated. The alumina coating seems to shifts the critical stress level to even higher values than the already high value (~1 GPa) required to support plasticity in uncoated Au ligaments.

In the field of catalysis, the critical questions is if ALD coatings can be used to further improve the catalytic properties of np-Au while adding thermal stability for high temperature applications. To answer this question we studied the thermal stability and catalytic activity of TiO_2-coated np-Au as it is known that the combination of Au and TiO_2 leads to highly active catalysts.[25] The development of the ligament size vs. annealing temperature is shown in Figure 2a, and representative morphology changes are shown in Figure 4. TiO_2 coatings also increase the thermal stability of np-Au, but less than the Al_2O_3 coatings discussed above. Annealing at 600 ^oC does only slightly increase the characteristic feature size of np-Au, but breaks up the initially continuous and smooth TiO_2 coating into highly dispersed nanoparticles (Fig. 4, top

panel). Above 600 ^{o}C, the ligaments of TiO_2-coated np-Au start to coarsen, but not as fast as those in uncoated np-Au. The thermal stability caused by metal oxide coatings seems to correlate better with the crystallization temperature (TiO_2: ~370 ^{o}C,[51] Al_2O_3: ~ 900-1000 ^{o}C[32, 33]) than with the melting point (TiO_2: ~ 1843 ^{o}C, Al_2O_3: ~2053 ^{o}C). The slower coarsening kinetics, and the serrated structure of TiO_2-coated np-Au annealed at or above 700 ^{o}C can be attributed to step edge pinning by TiO_2 nanoparticles that was also observed in Au single crystal experiments.[52]

The morphology of the TiO_2/Au nanocomposite structures that results from annealing is very interesting for catalytic applications. Indeed, first catalytic tests using the oxidation of CO, CO + ½ O_2 → CO_2, as a test reaction already demonstrate the potential of ALD functionalization to design new np-Au catalysts with improved catalytic activity and thermal stability (Fig. 5). Pristine TiO_2-coated np-Au is catalytically in-active as titania itself is not active for CO oxidation[53] and TiO_2 completely covers the np-Au surface. After annealing at 600 ^{o}C, however, TiO_2-coated np-Au shows an almost 3 times larger activity towards CO oxidation as compared to uncoated np-Au. In contrast, annealing of uncoated np-Au at 600 ^{o}C decreases its activity by more than 50 % which can be attributed to the loss of catalytically active surface area due to coarsening (see Fig. 2a). A comparison with Figure 4 reveals that annealing at 600 ^{o}C is sufficient to break up the initially continuous TiO_2 film into TiO_2 nanocrystals. The presence of these TiO_2 nanocrystals on the surface of the ligaments of np-Au likely increases the efficiency for O_2 dissociation as a source for atomic oxygen which is the rate limiting step for CO oxidation with gold based catalysts.[25] The TiO_2 coating also stabilizes the nanoscale structure of the material, and thus reduces the loss of catalytically active surface area during annealing/high temperature applications.

In conclusion, our results demonstrate that ALD functionalization offers an opportunity to drastically improve the thermal stability and mechanical properties of np-Au, and even increase the catalytic activity at the same time. For example, only one-nm-thick Al_2O_3 films can stabilize the nanoscale morphology of np-Au up to 1000°C, and ~6-nm-thick films lead to a 3- and 7-fold increase in Young's modulus and hardness, respectively, while increasing the density by only 10%. This also demonstrates that thin oxide films can have a pronounced effect on nanomechanical tests, and although np-Au itself is not a good choice for structural applications due to it's the high costs, our results demonstrate the potential of ALD coatings to improve the mechanical properties of other nanoscale materials, for example, for nanoelectromechanical systems (NEMS). Catalytic tests with TiO_2 coated np-Au also demonstrate that ALD surface functionalization can improve the catalytic activity of np-Au. For example, the presence of highly dispersed TiO_2 nanoparticles on Au ligaments, formed by annealing the initially smooth and continuous TiO_2 film at 600 ^{0}C, increases the catalytic activity towards CO oxidation by several hundred percent. The enhanced thermal stability combined with added functionally opens the door to many promising applications: For example, the plasmonic response of the nanoporous Au network[2, 10] allows for high temperature surface enhanced Raman spectroscopy.[54] The desired pore size can first be "dialed in" by annealing uncoated np-Au, and then be frozen in by applying a nm-thick ALD coating. Improved thermal, mechanical and catalytic properties also enable high temperature actuator and catalysis applications.[13, 43] Metal oxide coated nanoporous metals are also promising electrode materials for batteries and energy harvesting and conversion applications.

Acknowledgement. Work at LLNL was performed under the auspices of the U.S. DOE by LLNL under Contract DE-AC52-07NA27344. We gratefully acknowledge Prof. Andrea Hodge, University of Southern California, who provided polished samples for mechanical testing.

References:

1. Wittstock, A.; Zielasek, V.; Biener, J.; Friend, C. M.; Baumer, M. *Science* **2010,** 327, 319-322.
2. Dongqing, H.; Tingting, X.; Jixin, S.; Xiaohong, X.; Yi, D. *ChemCatChem* **2010,** 2, 383-386.
3. Ding, Y.; Chen, M. W. *MRS Bulletin* **2009,** 34, 569-576.
4. Jia, J.; Cao, L.; Wang, Z. *Langmuir* **2008,** 24, 5932-5936.
5. Xu, C. X.; Su, J. X.; Xu, X. H.; Liu, P. P.; Zhao, H. J.; Tian, F.; Ding, Y. *J. Am. Chem. Soc.* **2007,** 129, 42-43.
6. Zielasek, V.; Jurgens, B.; Schulz, C.; Biener, J.; Biener, M. M.; Hamza, A. V.; Bäumer, M. *Angew. Chem. Int. Ed.* **2006,** 45, 8241-8244.
7. Lang, X. Y.; Guo, H.; Chen, L. Y.; Kudo, A.; Yu, J. S.; Zhang, W.; Inoue, A.; Chen, M. W. *J. Phys. Chem. C.* **2010,** 114, 2600-2603.
8. Lang, X. Y.; Guan, P. F.; Zhang, L.; Fujita, T.; Chen, M. W. *Appl. Phys. Lett.* **2010,** 96, 073701.
9. Lang, X. Y.; Chen, L. Y.; Guan, P. F.; Fujita, T.; Chen, M. W. *Appl. Phys. Lett.* **2009,** 94, 213109.
10. Biener, J.; Nyce, G. W.; Hodge, A. M.; Biener, M. M.; Hamza, A. V.; Maier, S. A. *Adv. Mater.* **2008,** 20, 1211-1217.
11. Dixon, M. C.; Daniel, T. A.; Hieda, M.; Smilgies, D. M.; Chan, M. H. W.; Allara, D. L. *Langmuir* **2007,** 23, 2414-2422.
12. Kucheyev, S. O.; Hayes, J. R.; Biener, J.; Huser, T.; Talley, C. E.; Hamza, A. V. *Appl. Phys. Lett.* **2006,** 89, 053102.
13. Biener, J.; Wittstock, A.; Zepeda-Ruiz, L. A.; Biener, M. M.; Zielasek, V.; Kramer, D.; Viswanath, R. N.; Weissmuller, J.; Bäumer, M.; Hamza, A. V. *Nat. Mater.* **2009,** 8, 47-51.
14. Kramer, D.; Viswanath, R. N.; Weissmueller, J. *Nano Letters* **2004,** 4, 793-796.
15. Weissmüller, J.; Viswanath, R. N.; Kramer, D.; Zimmer, P.; Wuerschum, R.; Gleiter, H. *Science* **2003,** 300, 312-315.
16. Erlebacher, J.; Aziz, M. J.; Karma, A.; Dimitrov, N.; Sieradzki, K. *Nature* **2001,** 410, 450-453.
17. Erlebacher, J.; Sieradzki, K. *Scripta Mater.* **2003,** 49, 991-996.
18. Li, R.; Sieradzki, K. *Phys. Rev. Lett.* **1992,** 68, 1168-1171.
19. Kertis, F.; Snyder, J.; Govada, L.; Khurshid, S.; Chayen, N.; Erlebacher, J. *JOM* **2010,** 62, 50-56.
20. Biener, J.; Hodge, A. M.; Hayes, J. R.; Volkert, C. A.; Zepeda-Ruiz, L. A.; Hamza, A. V.; Abraham, F. F. *Nano Lett.* **2006,** 6, 2379-2382.
21. Snyder, J.; Asanithi, P.; Dalton, A. B.; Erlebacher, J. *Adv. Mater.* **2008,** 20, 4883-+.
22. Xu, C. X.; Wang, R. Y.; Chen, M. W.; Zhang, Y.; Ding, Y. *Phys. Chem. Chem. Phys.* **2010,** 12, 239-246.
23. Biener, J.; Wittstock, A.; Biener, M. M.; Nowitzki, T.; Hamza, A. V.; Baeumer, M. *Langmuir* **2010,** 26, 13736-13740.
24. Ge, X. B.; Yan, X. L.; Wang, R. Y.; Tian, F.; Ding, Y. *J. Phys. Chem. C.* **2009,** 113, 7379-7384.
25. Bond, G. C.; Thompson, D. T. *Gold Bull.* **2000,** 33, 41-51.
26. Baumann, T. F.; Biener, J.; Wang, Y. M. M.; Kucheyev, S. O.; Nelson, E. J.; Satcher, J. H.; Elam, J. W.; Pellin, M. J.; Hamza, A. V. *Chem. Mater.* **2006,** 18, 6106-6108.
27. Biener, J.; Baumann, T. F.; Wang, Y. M.; Nelson, E. J.; Kucheyev, S. O.; Hamza, A. V.; Kemell, M.; Ritala, M.; Leskela, M. *Nanotechnol.* **2007,** 18, 055303.
28. George, S. M. *Chem. Rev.* **2010,** 110, 111-131.
29. Lee, D.; Wei, X.; Chen, X.; Zhao, M.; Jun, S. C.; Hone, J.; Herbert, E. G.; Oliver, W. C.; Kysar, J. W. *Scripta Mater.* **2007,** 56, 437-440.
30. Qian, L. H.; Shen, W.; Das, B.; Shen, B.; Qin, G. W. W. *Chem. Phys. Lett.* **2009,** 479, 259-263.
31. Qian, L. H.; Shen, W.; Shen, B.; Qin, G. W. W.; Das, B. *Nanotechnol.* **2010,** 21, 305705.
32. Jakschik, S.; Schroeder, U.; Hecht, T.; Gutsche, M.; Seidl, H.; Bartha, J. W. *Thin Solid Films* **2003,** 425, 216-220.

33. Katamreddy, R.; Inman, R.; Jursich, G.; Soulet, A.; Nicholls, A.; Takoudis, C. *Thin Solid Films* **2007,** 515, 6931-6937.
34. Standridge, S. D.; Schatz, G. C.; Hupp, J. T. *Langmuir* **2009,** 25, 2596-2600.
35. Linsebigler, A. L.; Lu, G. Q.; Yates, J. T. *Chem. Rev.* **1995,** 95, 735-758.
36. Jia, C. C.; Yin, H. M.; Ma, H. Y.; Wang, R. Y.; Ge, X. B.; Zhou, A. Q.; Xu, X. H.; Ding, Y. *J. Phys. Chem. C.* **2009,** 113, 16138-16143.
37. Cheah, S. K.; Perre, E.; Rooth, M.; Fondell, M.; Hårsta, A.; Nyholm, L.; Boman, M.; Gustafsson, T.; Lu, J.; Simon, P.; Edström, K. *Nano Lett.* **2009,** 9, 3230-3233.
38. Robertson, J. *Rep. Prog. Phys.* **2006,** 69, 327-396.
39. Hodge, A. M.; Biener, J.; Hayes, J. R.; Bythrow, P. M.; Volkert, C. A.; Hamza, A. V. *Acta Mater.* **2007,** 55, 1343-1349.
40. Aarik, J.; Aidla, A.; Mändar, H.; Uustare, T. *Appl. Surf. Sci.* **2001,** 172, 148-158.
41. Groner, M. D.; Fabreguette, F. H.; Elam, J. W.; George, S. M. *Chem. Mater.* **2004,** 16, 639-645.
42. Oliver, W. C.; Pharr, G. M. *J. Mater. Res.* **1992,** 7, 1564-1583.
43. Kramer, D.; Viswanath, R. N.; Weissmüller, J. *Nano Lett.* **2004,** 4, 793-796.
44. Liu, X. W.; Hu, J.; Pan, B. C. *Physica E* **2008,** 40, 3042-3048.
45. Gibson, L. J.; Ashby, M. F., *Cellular Solids: Structure and Properties*. 2nd. ed.; Cambridge University Press: Cambridge, UK, 1997.
46. Biener, J.; Hodge, A. M.; Hamza, A. V.; Hsiung, L. M.; Satcher, J. H. *J. Appl. Phys.* **2005,** 97, 024301.
47. Hodge, A. M.; Doucette, R. T.; Biener, M. M.; Biener, J.; Cervantes, O.; Hamza, A. V. *J. Mater. Res.* **2009,** 24, 1600-1606
48. Kiely, J. D.; Houston, J. E. *Phys. Rev. B* **1998,** 57, 12588-12594.
49. Herrmann, C. F.; DelRio, F. W.; George, S. M.; Bright, V. M., Properties of atomic layer deposited Al2O3/ZnO dielectric films grown at low temperature for RF MEMS. In *Micromachining and Microfabrication Process Technology X*, Maher, M. A.; Stewart, H. D., Eds. 2005; Vol. 5715, pp 159-166.
50. Tripp, M. K.; Stampfer, C.; Miller, D. C.; Helbling, T.; Hermann, C. F.; Hierold, C.; Gall, K.; George, S. M.; Bright, V. M. *Sensors and Actuators A* **2006,** 130, 419-429.
51. Yin, S.; Inoue, Y.; Uchida, S.; Fujishiro, Y.; Sato, T. *J. Mater. Res.* **1998,** 13, 844-847.
52. Biener, J.; Farfan-Arribas, E.; Biener, M.; Friend, C. M.; Madix, R. J. *J. Chem. Phys.* **2005,** 123, 094705.
53. Diebold, U. *Surf. Sci. Rep.* **2003,** 48, 53-229.
54. Whitney, A. V.; Elam, J. W.; Stair, P. C.; Van Duyne, R. P. *J. Phys. Chem. C.* **2007,** 111, 16827-16832.

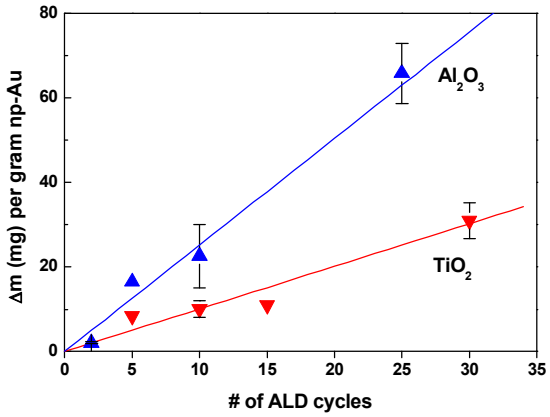

Figure 1: Normalized mass gain per gram np-Au vs. number of ALD cycles for both Al_2O_3 and TiO_2 deposition. The normalized mass gain increases approximately linear with the number of ALD cycles, and the growth rates are ~0.25 and ~0.07 nm per cycle for Al_2O_3 and TiO_2, respectively. Error bars indicate the standard deviation obtained from 3 or more individual coating experiments.

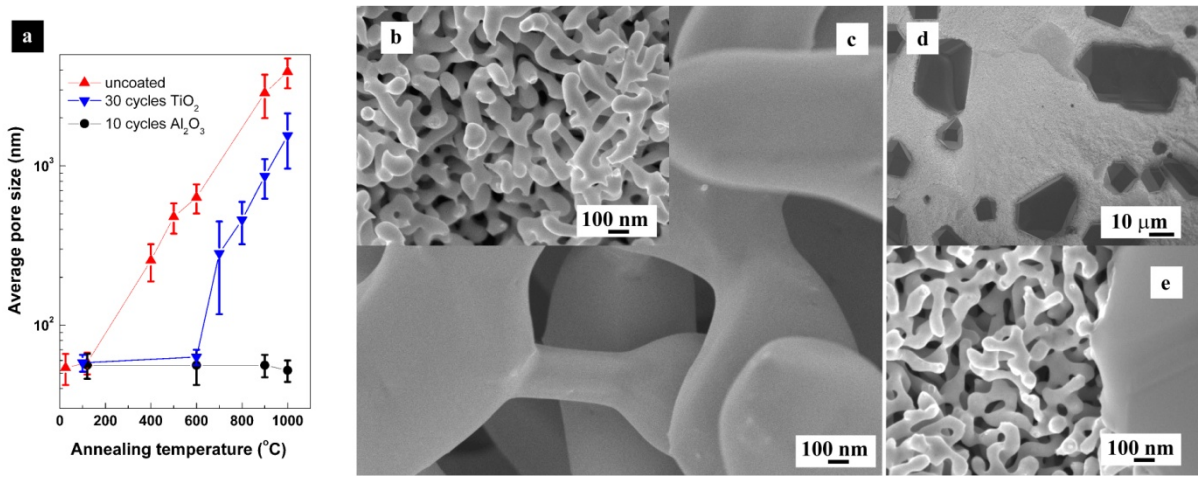

Figure 2: Thermal stability of Al_2O_3- and TiO_2-coated np-Au: (a) development of average ligament size of Al_2O_3- (10 cycles), TiO_2- (30 cycles), and un-coated np-Au vs. annealing temperature; SEM micrographs obtained from (b) Al_2O_3-coated (10 cycles) and (c) uncoated np-Au after annealing at 600 ^oC; (d-e) surface of an alumina-coated npAu sample after annealing at 1000 ^oC imaged at different magnifications. After annealing at 1000 ^oC, the surface is covered with micron-sized Au crystallites (d), but the nanoscale structure of np-Au is still intact (e).

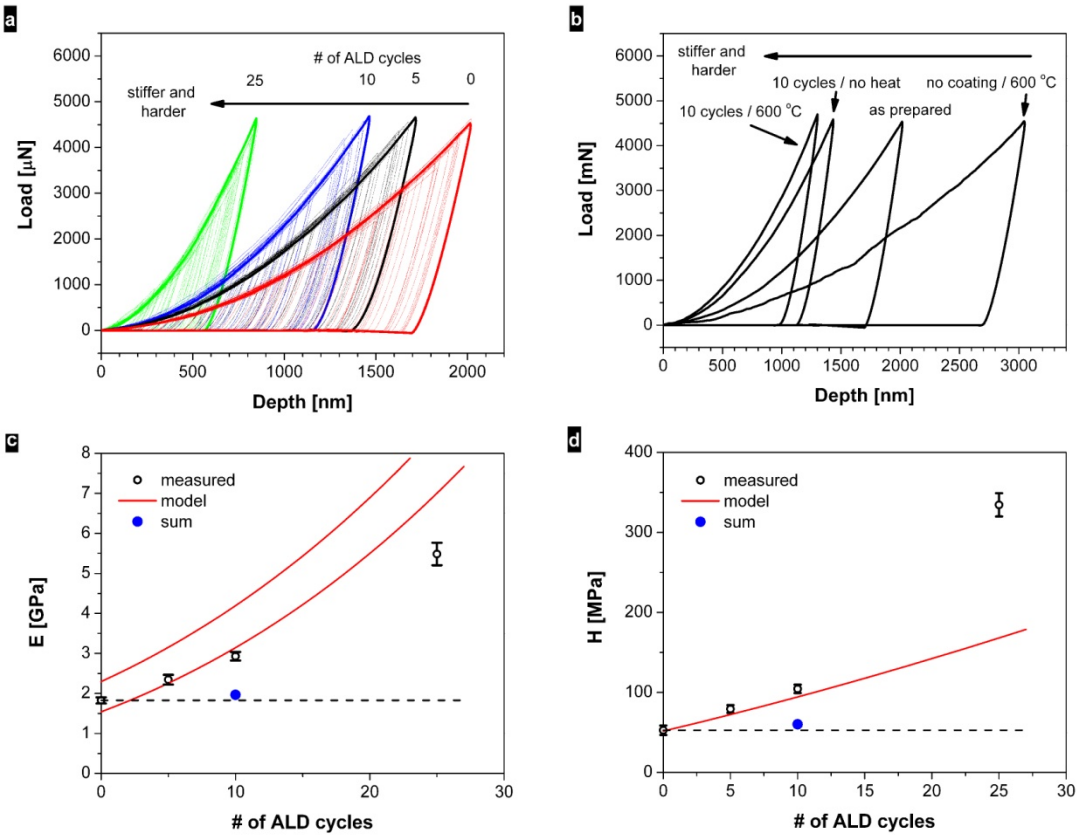

Figure 3: Mechanical properties of Al_2O_3-coated np-Au samples: (a) Nanoindentation load-displacement curves of np-Au samples coated with 0, 5, 10, and 25 ALD cycles, respectively. (b) Effect of annealing on the load-displacement nanoindentation curves for both coated (10 ALD cycles) and uncoated np-Au samples; Young's modulus (c) and Hardness (d) versus number of ALD cycles obtained from the nanoindentation data shown in (a), and values predicted by the core-shell model.

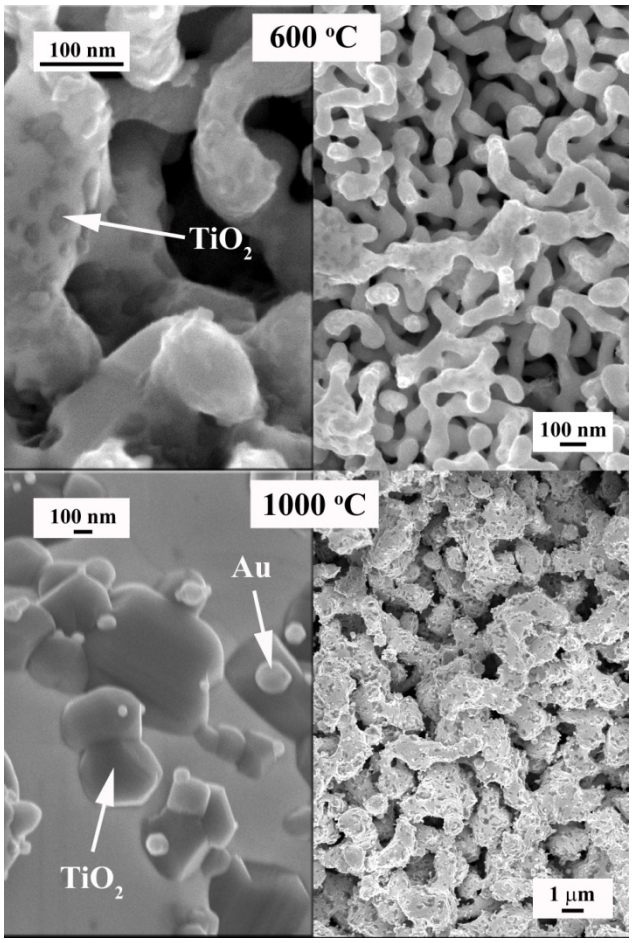

Figure 4: SEM micrographs showing representative morphological changes of TiO_2-coated (30 cycles) np-Au films upon annealing at 600 ^oC (top) and 1000 ^oC (bottom), respectively. Annealing at 600 ^oC does only slightly increase the characteristic feature size of np-Au (see also figure 2a), but breaks up the initially continuous and smooth TiO_2 coating (not shown) into highly dispersed nanoparticles (top panel). Coarsening of the Au ligaments is observed during annealing at or above 700 ^oC. At 1000 ^oC, for example, this leads to the formation of micron-sized ligaments decorated with well-facetted TiO_2 crystals that are sometimes decorated with Au nano-crystals. Elemental composition of the different features was verified with area-specific EDAX.

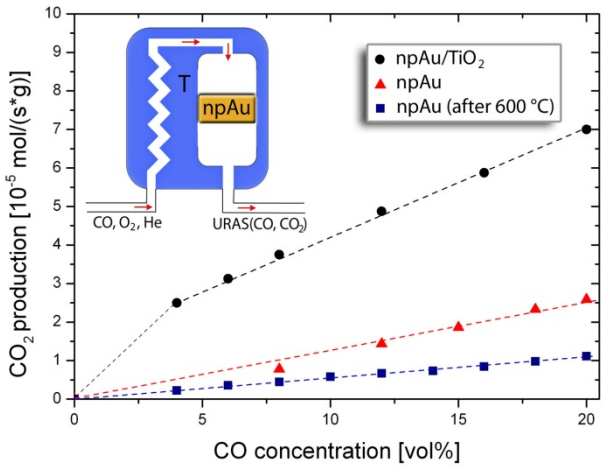

Figure 5:.Comparison of the catalytic activity of a TiO_2 modified (10 ALD cycles/annealed at 600 ^oC) np-Au sample with an uncoated np-Au sample before and after annealing a 600 ^oC in He. Shown is the catalytic activity towards CO oxidation measured at 60 °C using 4-20 vol. % CO and 30 vol. % O_2 in a He carrier gas. Titania-coating causes a 3-fold increase in the catalytic activity with respect to the uncoated, not annealed np-Au sample, while annealing of the uncoated np-Au sample at 600 ^oC decreases its reactivity by more than 50 %.